American Journal of Engineering Research (AJER)
e-ISSN: 2320-0847 p-ISSN : 2320-0936
Volume-6, Issue-10, pp-259-271
www.ajer.org
Research Paper Open Access

Modeling and Analysis of Floating-Ring Bearing Thermo-Hydrodynamic Parameters for Advanced Turbo-Rotor Systems

Daniel Tamunodukobipi[a*]. Ibiba Emmanuel-Douglas[a]. Yong-Bok Lee[b]
[a]*Department of Marine Engineering, Rivers State University of Science and Technology, Port Harcourt, Nigeria,*
[b]*Energy Mechanics Resource Center, Korea Institute of Science and Technology, 39-1 Hawolgok-dong, Songbuk-gu, Seoul, 136-791, Korea*
[*]*Corresponding author: Tel.: +234(0)805 439 9401*

ABSTRACT: *This work presents a detailed analysis and modeling of floating-ring bearings (FRBs) for predicting their dynamic-force coefficients, thermo-hydrodynamic characteristics, and instability behavior. The mathematical model is based on modified Reynolds equations combined with thermo-viscous and centrifugal-force effects. The force coefficients are obtained from the non-linear integration of film pressures using Sommerfeld integrals. The results display the impacts of film properties and journal speed on load capacity, rotor eccentricity, viscous-friction, and whirl frequency. Also, the relationship between FRB geometry (radius ratio, R_2/R_1; slenderness, L/D_2; and clearance ratio, C_2/C_1) and load capacity, oil-flow, and heat dissipation are established. Predictions agree with test-data.*
Key Words: *floating-ring bearing; dynamic coefficients; rotor-bearing system, turbochargers, analytical modeling of oil-bearings.*

Date of Submission: 24-08-2017 Date of acceptance: 18-10-2017

I. BACKGROUND FOR THEORETICAL FORMULATION

There is an astronomical increase in rotor-bearing modeling nowadays with the advent of micro-computers and advances in numerical and computational techniques. Various models for predicting FRB dynamic force coefficients, instability behavior and energy loss have been developed for both design and off-design conditions [1-9]. Generally, predictive models are very essential because they are swifter, cost effective, more adaptive and highly efficient tools for bearing design, performance characterization and faults diagnosis [2, 3]. Furthermore, most contemporary bearings exhibit properties which are intrinsically interdependent but diversely influenced by changes in operating conditions. Their film parameters are so intertwined that the contributory effect of an individual parameter cannot be separately investigated experimentally. In such situations, the use of predictive tools becomes imperative as a lone solution for detailed parametric study of bearing properties considered individually or in conjunction with other parameters. Again, the reliability of experimentally identified FRB dynamic parameters is sometimes undermined by subsynchronous instability, properties non-linearity, electromagnetic noise, and improper mounting of sensors [3, 6-10]. These setbacks need pragmatic solutions which must be user friendly, economically viable and technically reliable for advanced turbo rotor-bearing design and parametric study. However, only a limited number of papers are published in this area.

Therefore, this work presents a comprehensive modeling of FRB thermo-hydrodynamic properties for application in high-speed turbomachinery. Modified Reynolds equations combined with thermo-viscous and centrifugal-force parameters are employed. The force coefficients are obtained from a piecewise, non-linear integration of film pressures using Sommerfeld integrals. Equations for oil flow, film temperatures, whirl-frequency ratio, ring-speed ratio and eccentricity ratio are developed and implemented. Physical explanations are given on the model predictions to show the practical significance of the results. Graphically comparison of predictions against veritable test data validates model's reliability.

II. PREVIOUS CONTRIBUTIONS

Floating-ring bearing (FRB) is a hydrodynamic bearing having a cylindrical metal ring (floating-ring) which is loosely fitted between the journal and the bearing housing. The ring becomes fluid borne on spinning under viscous shear to form two parallel hydrodynamic oil-films that act in series [1-3]. Figure 1 displays descriptive schematics of a full floating-ring bearing (FRB) used in supporting rotors of most high-speed turbomachinery.

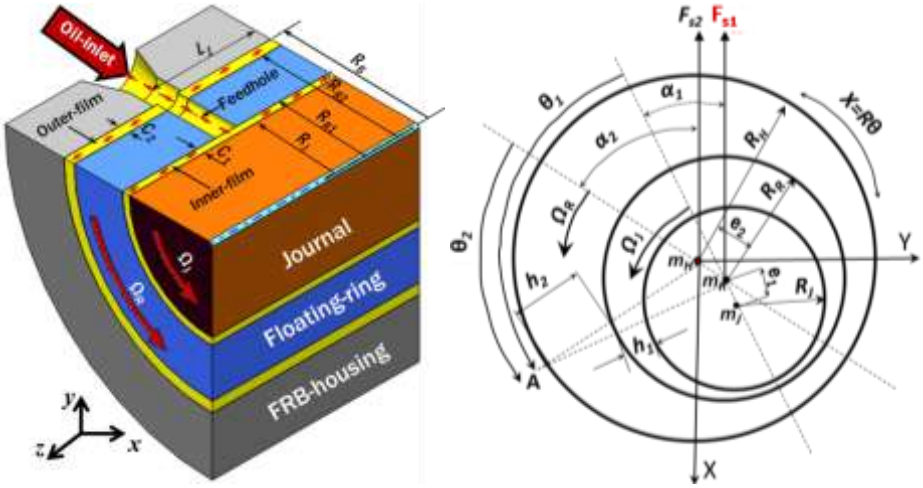

(a) **(b)**

Fig. 1: FRB schematics: (a) section view of assemblage, (b) free-body diagram

The constitutive Reynolds equations in polar coordinates for the inner and the outer films are given in Eqs. (1) and (2), respectively, [7, 8]. Chow [7] and Orcutt and Ng [8], using these Reynolds equations, performed analysis for FRB dynamic force coefficients at steady-state and with pressurized oil supply. Sixteen linearized dynamic force parameters from the two oil-films were obtained and subsequently condensed to the standard eight non-dimensional force coefficients by implementing force balancing technique. However, their theoretical results were not calibrated or complemented by test data.

$$\frac{\partial}{R_1\partial\theta_1}\left(\frac{h_1^3}{\mu_1}\frac{\partial P_1}{R_1\partial\theta_1}\right)+\frac{\partial}{\partial Z}\left(\frac{h_1^3}{\mu_1}\frac{\partial P_1}{\partial Z}\right)=6(\Omega_J+\Omega_R)\frac{\partial h_1}{\partial\theta_1}+6h_1\frac{\partial}{\partial\theta_1}(\Omega_J+\Omega_R)+12\frac{\partial h_1}{\partial t} \quad (1)$$

$$\frac{\partial}{R_2\partial\theta_2}\left(\frac{h_2^3}{\mu_2}\frac{\partial P_2}{R_2\partial\theta_2}\right)+\frac{\partial}{\partial Z}\left(\frac{h_2^3}{\mu_2}\frac{\partial P_2}{\partial Z}\right)=6\Omega_R\frac{\partial h_2}{\partial\theta_2}+6h_2\frac{\partial}{\partial\theta_2}\Omega_R+12\frac{\partial h_2}{\partial t} \quad (2)$$

So, Tamunodukobipi, et al [3, 9] and Tatara [5] conducted experiments to characterize FRB dynamic force coefficients and ring speed ratio, respectively: and reported that despite the excellent damping properties of FRBs, they still exhibit two distinct regions of instability. It was also noted that FRBs testing is clumsy, expensive and often flawed by measurement errors. The poor test-data quality was attributed to signal noise, sensor mounting defects, and subsynchronous instability. Thus, the evolving and use of virtual predictive tools is favoured.

Consequently, Tanaka, et al [11] developed a hydrodynamic model with film cavitation to predict the rotordynamic coefficients and ring-speed ratio of lightly loaded FRBs operating at very high shaft speeds. Their results indicated a decrease of FRB cross-coupling stiffness with increasing inner oil-film rupture at higher shaft speeds. Koeneke, et al [12] opined that the film rupture in FRBs was due mainly to centrifugal repulsion of lubricant by the rotor. However, Clarke, et al [13] using thermal model showed that bubbles in the inner film were thermally induced and originated from the liquid-solid interfaces: and hence, argued that film rupture at elevated speeds should rather be due to high temperature. Probing the thermal characteristics of FRBs, Shaw and Nussdorfer [1] analyzed the bearing losses and thermal management effectiveness of FRB in comparison with those of a single-film journal-bearing (SFJB) of equivalent dimensions. It was found that FRBs have lesser friction loss and better convective flow than SFJBs; even though the latter have higher load capacities than the double-film bearings. San Andrés and Kerth [10] investigated the thermal effects on the performance of FRB-

supported turbocharger (*TC*) rotor system. The researchers estimated the FRB dynamic load capacity, ring speed ratio and instability.

While lauding the efforts of previous authors, this work, however, develops and implements a novel model to characterize FRB load capacity, ring speed ratio, rotor eccentricity, oil flow-rate, film temperature and energy loss. It predicts these parameters and compares them against those of an equivalent SFJB. In this paper, several thermo-hydrodynamic equations are synthesized, implemented and their results benchmarked against test data for validation.

III. ANALYSIS OF *FRB* FORCE PARAMETERS AND RING SPEED-RATIO

In Figure 2, FRB dynamic force coefficients and rotor eccentricities are illustrated. The eccentricity triangle shows $\boldsymbol{e_1}$ and $\boldsymbol{e_2}$ that represent the journal and floating-ring eccentricities from their respective centers. The symbols (m_H, m_J, m_R) are the masses of the housing, journal and ring, respectively.

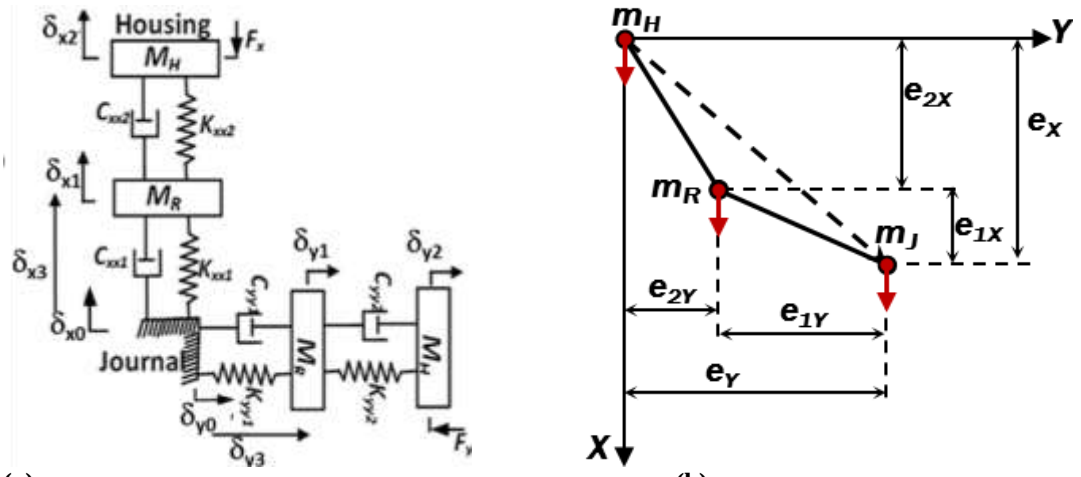

Fig. 2: Description of FRB (a) force components, and (b) eccentricity triangle

The Reynolds equation for the inner film can be rewritten as defined in Eq. (3). This modification is imperative because hydrodynamic wedge develops only where there is relative velocity $(\Omega_J - \Omega_R)$. The inner film force-coefficients predicted by Eq. (1) having $(\Omega_J + \Omega_R)$ are too large for FRB test data: and even larger than those of a SFJB with equivalent film-clearance.

$$\frac{\partial}{R_1 \partial \theta_1}\left(\frac{h_1^3}{\mu_1}\frac{\partial P_1}{R_1 \partial \theta_1}\right) + \frac{\partial}{\partial Z}\left(\frac{h_1^3}{\mu_1}\frac{\partial P_1}{\partial Z}\right) = 6(\Omega_J - \Omega_R)\frac{\partial h_1}{\partial \theta_1} + 6h_1\frac{\partial}{\partial \theta_1}(\Omega_J - \Omega_R) + 12\frac{\partial h_1}{\partial t} \qquad (3)$$

A forensic investigation with identical gas bump-foil journal bearings (GBFJBs) reveals that the rotor on the GBFJB with fixed top-foil lifted at 6.0 krpm, while that on the loose top-foil never lifted even at 12 krpm [14]. Figure 3 illustrates the hydrodynamic wedge conditions in SFJB, FRB and hypothetical bearings having a zero relative velocity.

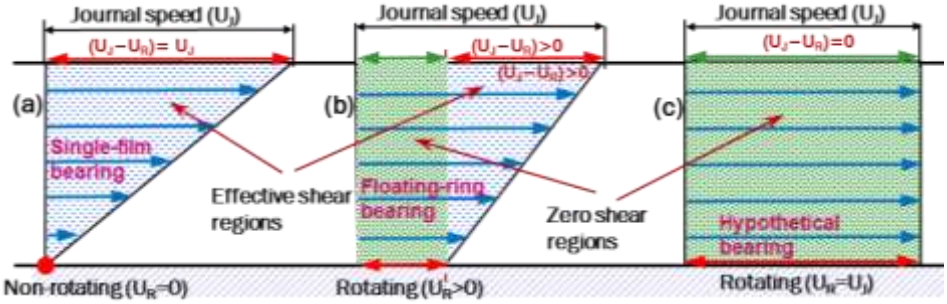

Fig. 3: Illustrative drawing of film shear in different journal configurations: (a) SFJB, (b) FRB and (c) Hypothetical

In the instance of the same journal speed, the hydrodynamic force is greater in (a) SFJB than in (b) FRB, but zero in (c) the hypothetical case because $(\Omega_J - \Omega_R) = 0$. The modified Reynolds equation agrees well with the physics of hydrodynamics of JBs [15]. Note that the self-generated film-pressure is always proportional to the shear strain across the fluid body.

3.1 Modeling Ring Speed, Eccentricity and Viscosity

By this modification and assuming the short-bearing theory, the Sommerfeld numbers for the inner and the outer films are defined, respectively, by Eqs. (4) and (5).

$$Sn_1 = \frac{\mu_1(\Omega_J - \Omega_R)LD_1}{W}\left(\frac{R_1}{c_1}\right)^2 = \frac{\left(1-\varepsilon_1^2\right)^2}{\pi\varepsilon_1\sqrt{16\,\varepsilon_1^2 + \pi^2\left(1-\varepsilon_1^2\right)}} \tag{4}$$

$$Sn_2 = \frac{\mu_2\Omega_R LD_2}{W}\left(\frac{R_2}{c_2}\right)^2 = \frac{\left(1-\varepsilon_2^2\right)^2}{\pi\varepsilon_2\sqrt{16\,\varepsilon_2^2 + \pi^2\left(1-\varepsilon_2^2\right)}} \tag{5}$$

To calculate the individual films' load-capacities, it is pertinent to predetermine the speeds and eccentricities of the ring and journal, respectively. Thus, from Eqs. (4) and (5), the ring-to-journal speed ratio (β) is derived as given in Eq. (7): where ($\varepsilon_1 = e_1/c_1$) and ($\varepsilon_2 = e_2/c_2$).

$$\frac{Sn_2}{Sn_1} = \frac{\Omega_R}{(\Omega_J - \Omega_R)}\left(\frac{\mu_2}{\mu_1}\right)\left(\frac{P_1}{P_2}\right)\left(\frac{c_1}{c_2}\right)^2\left(\frac{R_2}{R_1}\right)^3 = \lambda_s\left(\frac{\varepsilon_1}{\varepsilon_2}\right)\left(\frac{1-\varepsilon_2^2}{1-\varepsilon_1^2}\right)^2\sqrt{\frac{16\,\varepsilon_1^2 + \pi^2\left(1-\varepsilon_1^2\right)}{16\,\varepsilon_2^2 + \pi^2\left(1-\varepsilon_2^2\right)}}$$

$$\frac{\beta}{(1-\beta)}\left(\frac{\mu_2}{\mu_1}\right)\left(\frac{c_1}{c_2}\right)^2\left(\frac{P_1}{P_2}\right)\left(\frac{R_2}{R_1}\right)^3 = \lambda_s\left(\frac{\varepsilon_1}{\varepsilon_2}\right)\left(\frac{1-\varepsilon_2^2}{1-\varepsilon_1^2}\right)^2\sqrt{\frac{16\,\varepsilon_1^2 + \pi^2\left(1-\varepsilon_1^2\right)}{16\,\varepsilon_2^2 + \pi^2\left(1-\varepsilon_2^2\right)}} \tag{6}$$

$$\beta = \left\{\frac{\lambda_\beta\left(\frac{\varepsilon_1}{\varepsilon_2}\right)\left(\frac{1-\varepsilon_2^2}{1-\varepsilon_1^2}\right)^2\sqrt{\frac{16\,\varepsilon_1^2 + \pi^2\left(1-\varepsilon_1^2\right)}{16\,\varepsilon_2^2 + \pi^2\left(1-\varepsilon_2^2\right)}}}{\left(\frac{\mu_2}{\mu_1}\right)\left(\frac{P_1}{P_2}\right)\left(\frac{c_1}{c_2}\right)^2\left(\frac{R_2}{R_1}\right)^3 + \left(\frac{\varepsilon_1}{\varepsilon_2}\right)\left(\frac{1-\varepsilon_2^2}{1-\varepsilon_1^2}\right)^2\sqrt{\frac{16\,\varepsilon_1^2 + \pi^2\left(1-\varepsilon_1^2\right)}{16\,\varepsilon_2^2 + \pi^2\left(1-\varepsilon_2^2\right)}}}\right\} \tag{7}$$

From Ref. [4], the inner and outer torques are defined by Eqs. (8). At steady-state, $\tau_2 = \lambda_\tau\tau_1$, which yields an expression for β. By inserting Eq. (9) into Eq. (6) and solving out yields the eccentricity relation of Eq. (10). The solution for ε_2 is obtainable by roots finding algorithm.

$$\left.\begin{aligned}\tau_1 &= \frac{2\pi\mu_1 L_1 R_1^3(\Omega_J - \Omega_R)}{c_1\sqrt{1-\varepsilon_1^2}}\\ \tau_2 &= \frac{2\pi\mu_2 L_2 R_2^3\Omega_R}{c_2\sqrt{1-\varepsilon_2^2}}\end{aligned}\right\} \tag{8}$$

$$\frac{\beta}{1-\beta} = \lambda_\tau\frac{\mu_1}{\mu_2}\frac{c_2}{c_1}\left(\frac{R_1}{R_2}\right)^3\sqrt{\frac{1-\varepsilon_2^2}{1-\varepsilon_1^2}} \tag{9}$$

$$\varepsilon_2\frac{\sqrt{16\,\varepsilon_2^2 + \pi^2\left(1-\varepsilon_2^2\right)}}{\left(1-\varepsilon_2^2\right)^{1.5}} = \lambda_\varepsilon\varepsilon_1\left(\frac{P_2}{P_1}\right)\left(\frac{c_2}{c_1}\right)\frac{\sqrt{16\,\varepsilon_1^2 + \pi^2\left(1-\varepsilon_1^2\right)}}{\left(1-\varepsilon_1^2\right)^{1.5}} \tag{10}$$

The symbols (μ_1, μ_2) denote the effective viscosities of the inner and outer films, respectively; whereas (λ_β, λ_ε, λ_τ) designate the correlation factors for the speed-ratio, eccentricity-ratio and torque-ratio, respectively. The film viscosity is a temperature dependent variable computed from Vogel's equation.

$$\mu = \left\{\mu_\infty - \frac{\mu_\infty - K\,e^{a/(b+T)}}{\left(\dot{\gamma}/\dot{\gamma}_c\right)}\right\} \tag{11}$$

Where μ_∞ represents reference viscosity at null shear rate; while *K*, *a* and *b* are Vogel' thermo-viscous fitting parameters to be determined experimentally. The symbols ($\dot{\gamma}$ and $\dot{\gamma}_c$) are the shear rate and the shear rate that produces 50% reduction in reference viscosity, respectively. The whirl frequency ratio (*WFR*) is estimated using Eq. (12):

$$WFR = \frac{I_P}{I_T}\beta = \frac{4\left(1+\left(\frac{R_2}{R_1}\right)^2\right)}{4\left(\frac{L}{D_1}\right)^2 + 3\left(1+\left(\frac{R_2}{R_1}\right)^2\right)}\beta \qquad (12)$$

where $I_P = \frac{m_R}{3}\left(R_1^2 + R_2^2\right)$ and $I_T = \frac{m_R}{12}\left[3\left(R_1^2 + R_2^2\right) + L^2\right]$ are the polar and transverse moments of inertia, respectively. Having known the relations for speed, eccentricity, whirl frequency ratio and Sommerfeld numbers: next is to develop a procedure for obtaining FRB equivalent force parameters.

3.2 Coefficients Summation Procedure by Superposition

Let the governing equations of motions and forces on the bearing housing (*H*) and the floating ring (*R*) about their respective steady-state equilibrium positions (*SSEP*) be:

$$\begin{aligned} M_H\ddot{\delta}_H + C_2\dot{\delta}_{HR} + K_2\delta_{HR} &= F_{ext(t)} \\ M_R\ddot{\delta}_R + C_1\dot{\delta}_{RJ} + K_1\delta_{RJ} &= C_2\dot{\delta}_{HR} + K_2\delta_{HR} \end{aligned} \qquad (13)$$

The Fourier solutions to the second order differential equations of the dynamic system are given in Eqs. (14). As indicated in Figure 2(a), the symbols (*M*, *K*, *C*) are the 2-by-2 matrices of the inertia, stiffness and damping coefficients; while the notations (F_{ext}, δ) represent the 2-by-2 matrices of the external exciting forces and the corresponding displacements from *SSEP*, respectively. The single and double dots over any symbol(s) denote the first and the second order time derivatives, respectively. Subscripts (*H, J, R*) stand for the housing, journal, and the ring, respectively; whereas (*HJ, HR, RJ*) represent their relative perturbation distances from each other. The notations (ω, *t*) represent the excitation frequency and time, respectively.

$$\begin{aligned} -\omega^2 M_H\delta_H + (K_2 + i\omega C_2)\delta_{HR} &= F_{ext(\omega)} \\ -\omega^2 M_R\delta_R + (K_1 + i\omega C_1)\delta_{RJ} &= (K_2 + i\omega C_2)\delta_{HR} \end{aligned} \qquad (14)$$

Assume that the journal has no lateral displacements ($\delta_{Jx} = \delta_{Jy} = 0$); then $\delta_R = \delta_{RJ}$ and $\delta_H = \delta_{HJ}$. Thus, $\delta_H = (\delta_{HR} + \delta_{RJ})$, and Eqs. (14) are rewritten as

$$\begin{aligned} -\omega^2 M_H\delta_{RJ} + \left(K_2 - \omega^2 M_H + i\omega C_2\right)\delta_{HR} &= F_{ext(\omega)} \\ \left(K_1 - \omega^2 M_R + i\omega C_1\right)\delta_{RJ} &= (K_2 + i\omega C_2)\delta_{HR} \end{aligned} \qquad (15)$$

Define the dynamic stiffness as $D_{(\omega)} = \left(K - \omega^2 M + i\omega C\right)$: then, Eqs. (15) become

$$\begin{aligned} -\omega^2 M_H\delta_{RJ} + D_{2(\omega)}\delta_{HR} &= F_{ext(\omega)} \\ D_{1(\omega)}\delta_{RJ} - (K_2 + i\omega C_2)\delta_{HR} &= 0 \end{aligned} \qquad (16)$$

From Eqs. (16), the mean displacements for the inner and outer films are derived as presented in Eqs. (17). The two equations of (17) are subsequently superposed to yield the overall displacement as given in Eq. (18). Dividing through by $F_{ext(\omega)}$ produces the flexibility matrix $\left[H^{eq}_{(\omega)}\right]$ as expressed in Eq. (19). The inverse of the flexibility matrix $\left[H^{eq}_{(\omega)}\right]$ generates the required FRB equivalent dynamic stiffness matrix $\left[D^{eq}_{(\omega)}\right]$ as presented in Eq. (20). It is pertinent to remark here that Eqs. (18) and (19) are valid for FRBs as well as squeeze-film dampers.

$$\begin{aligned} \delta_{RJ} &= \left[D_{1(\omega)}\right]^{-1}(K_2 + i\omega C_2)\delta_{HR} \\ \delta_{HR} &= \left(D_{2(\omega)} - \omega^2 M_H\left[D_{1(\omega)}\right]^{-1}(K_2 + i\omega C_2)\right)^{-1} F_{ext(\omega)} \end{aligned} \qquad (17)$$

$$\delta_{HJ} = \frac{\left[I + \frac{K_2 + i\omega C_2}{D_{1(\omega)}} \right]}{\left(D_{2(\omega)} - \frac{\omega^2 M_H \left(K_2 + i\omega C_2 \right)}{D_{1(\omega)}} \right)} F_{ext(\omega)} \qquad (18)$$

$$\left[H^{eq}_{(\omega)} \right] = \frac{\left[\delta_{HJ} \right]}{\left[F_{ext(\omega)} \right]} = \frac{\left[I + \frac{K_2 + i\omega C_2}{D_{1(\omega)}} \right]}{\left(D_{2(\omega)} - \frac{\omega^2 M_H \left(K_2 + i\omega C_2 \right)}{D_{1(\omega)}} \right)} \qquad (19)$$

$$\begin{bmatrix} D^{eq}_{yy} & D^{eq}_{xy} \\ D^{eq}_{yx} & D^{eq}_{xx} \end{bmatrix} = \frac{\begin{bmatrix} H^{eq}_{yy} & -H^{eq}_{xy} \\ -H^{eq}_{yx} & H^{eq}_{xx} \end{bmatrix}}{\left(H^{eq}_{xx} H^{eq}_{yy} - H^{eq}_{xy} H^{eq}_{yx} \right)} \qquad (20)$$

IV. MODEL IMPLEMENTATION PROCEDURE

Equations (2) and (3) for π-film short bearing are integrated numerically using Sommerfeld integrals to produce the non-dimensional force coefficients for the outer and inner films, respectively, [16-18]. The resulting 16 non-dimensional quantities are condensed by applying the superposition procedure using Eqs. (19) and (20) to yield the required 8 equivalent force parameters for FRB. Since the parameters are non-dimensional and functions of eccentricities, Eq. (10) is exploited to generate values of ε_2 for corresponding values of ε_1. The ring speed ratio is computed from Eq. (7); while the Sommerfeld numbers are computed from Eqs. (4) and (5). The effective film viscosities (μ_1, μ_2) as input variables are determined by thermal analysis for each journal-speed using Vogel's model. The quantity (*WFR*) is computed using Eq. (12). In rotor-bearing analysis, the *WFR* is considered as a rotordynamic instability indicator. The program execution flow chart is provided in Figure 4.

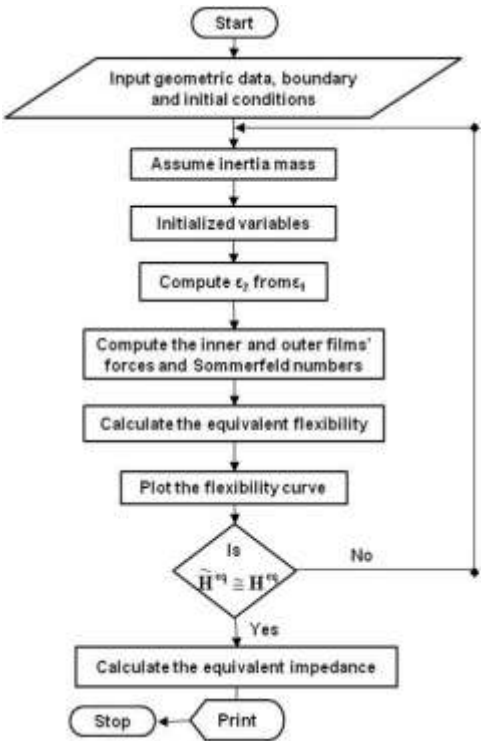

Fig. 4: Flow chart for predicting FRB dynamic force coefficients by superposition

V. MODEL PREDICTIONS

5.1 Predictions for Eccentricities and Ring-to-Journal Speed Ratios

Figure 5 displays the curves of floating-ring eccentricity (ε_2) versus journal eccentricity (ε_1) for different clearance ratios (c_2/c_1). Given that P_2/P_1=1.0 and λ_ε=1.0, the ring eccentricity is a polynomial curve which gradually becomes linearly proportional to the journal eccentricity at lower values of Sn_1 (i.e. $\varepsilon_1 \rightarrow 1$). Journal eccentricity is a function of bearing load and hydrodynamic film stiffness. So, correctly estimating the values of ε_1 and ε_2 is a prerequisite for proper characterizing of FRB stability and load capacity.

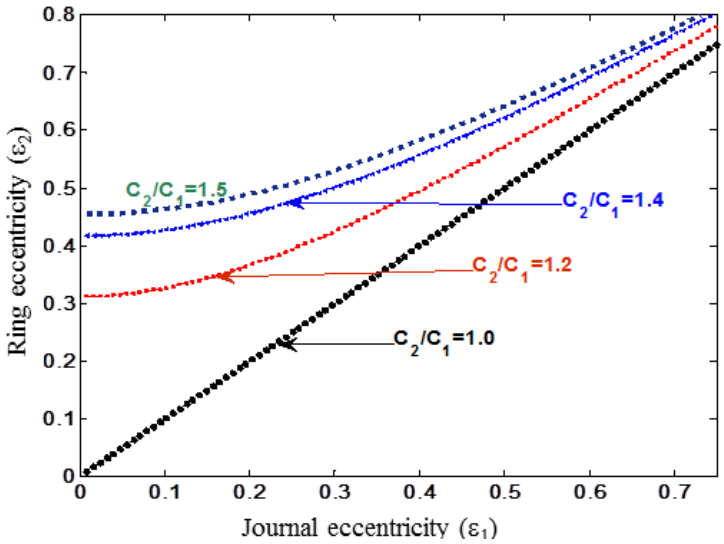

Fig. 5: Ring eccentricity for various values of clearance ratio and journal eccentricity

In Figures 6(a) to (c), the ring-speed ratio dependency on clearance, radius and viscosity ratios is independently investigated at different Sommerfeld numbers (Sn_1). It is found that ring speed ratio reduces with increasing journal speed (i.e. higher Sn_1). However, this phenomenon is uniquely influenced at different rates by the clearance ratio as in Figure 6(a), radius ratio as in Figure 6(b) and viscosity ratio as in Figure 6(c). In Figure 6(a), the ring speed ratio (N_R/N_J) is weakly affected by the changes in c_2/c_1; but substantially by the decrease in inner-film viscosity due to an increase in film temperature at higher Sommerfeld number (Sn_1) as evident in Figure 6(c). The N_R/N_J drops sharply from 0.5 to 0.15 as the Sn_1 value is raised. High Sn_1 value implies increased thermo-viscous energy dissipation in the inner film resulting in lower μ_2/μ_1. Consequently, the accelerating torque on the ring's inner-surface becomes weaker than its outer-surface drag torque: thus, produces a net retarding effect. Recall that torque due to shear force is directly proportional to the effective film-viscosity.

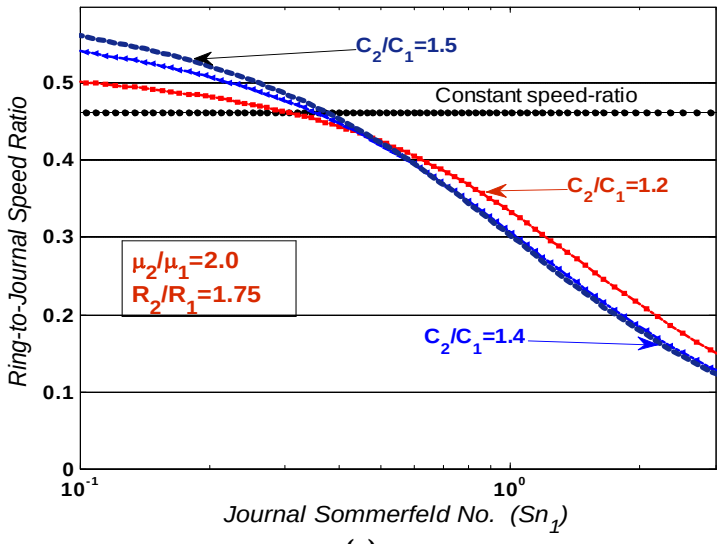

(a)

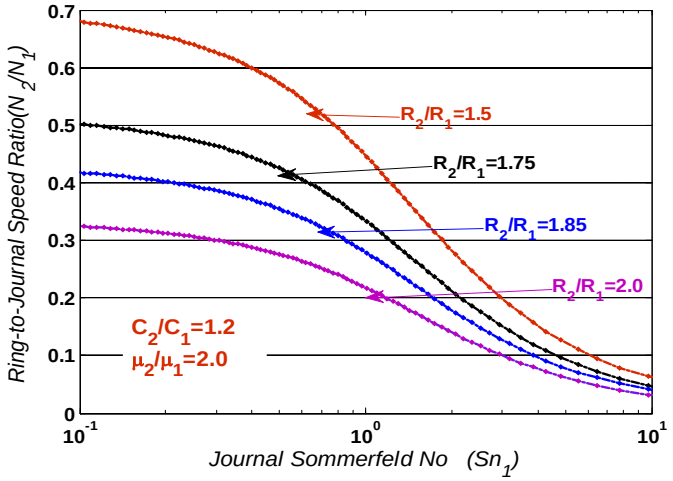

(b)

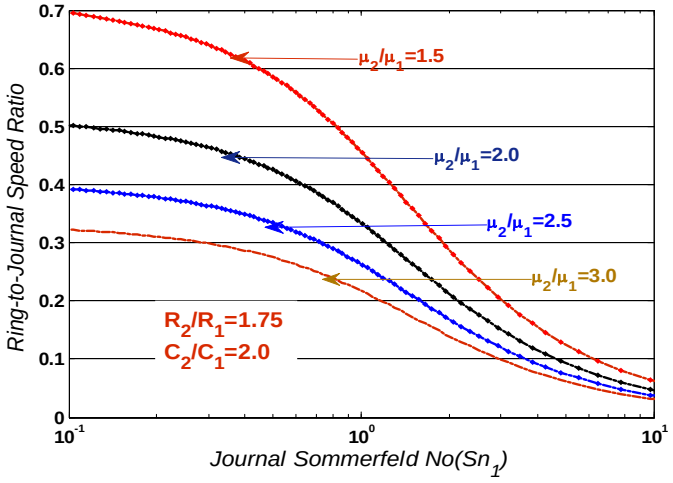

(c)

Fig. 6: Ring speed ratio for various values of (a) clearance ratio, (b) radius ratio, and (c) viscosity ratio at different journal Sommerfeld numbers

Similarly, in Figure 6(b), the response of N_R/N_J to change in R_2/R_1 is enormous, particularly at low Sn_1; but grows lesser at higher Sn_1, when thermo-viscous effect predominates. The characteristic decrease of N_R/N_J due to a larger R_2/R_1 is attributed to the greater inertia of the floating-ring acting to resist the accelerating torque. Typically, the ring's inertia is proportional to its mass. Nevertheless, if R_2/R_1 is constant, then N_R/N_J is affected essentially by the variation in μ_2/μ_1, since the latter is exponentially related to the film temperature. In practice, the value of μ_2/μ_1 is further reduced by the occurrence of bubbly lubricant in the inner film at high Sn_1. Therefore, while the effects of R_2/R_1 and c_2/c_1 on N_R/N_J grow lesser as Sn_1 increases, that of μ_2/μ_1 becomes larger as a result of thermo-viscous thinning of μ_1. Hence, N_R/N_J of a lightly loaded, high-speed turbomachinery depends principally on μ_2/μ_1.

5.2 Predictions for Whirl Frequency Ratio and Rotordynamic Instability

In Figures 7(a) and (b), the whirl frequency ratio (*WFR*) is higher for short bearings with slenderness ratio $L/D \leq 0.5$, and at lower Sn_1 than for large Sn_1 and long bearings with $L/D \geq 1.0$. This suggests that FRB susceptibility to instability is higher with short-width, low-speed bearings than the long-width, high-speed types. That is, rotordynamic stability improves with long-width FRB: thus, justifying the predominant use of long-width FRB for TCs. Furthermore, raising the value of c_2/c_1 causes a corresponding rise in *WFR*. That means a poorer stability performance. Nonetheless, at very high Sn_1, the negative effects of (c_2/c_1) and (L/D_1) on rotordynamic stability are insignificant. This elucidates the characteristic high stability performance of FRBs at elevated speeds ($Sn_1 \rightarrow \infty$) regardless of the values of c_2/c_1 and L/D_1. To be precise, $WFR < 0.5$ indicates a more stable rotor-bearing unit.

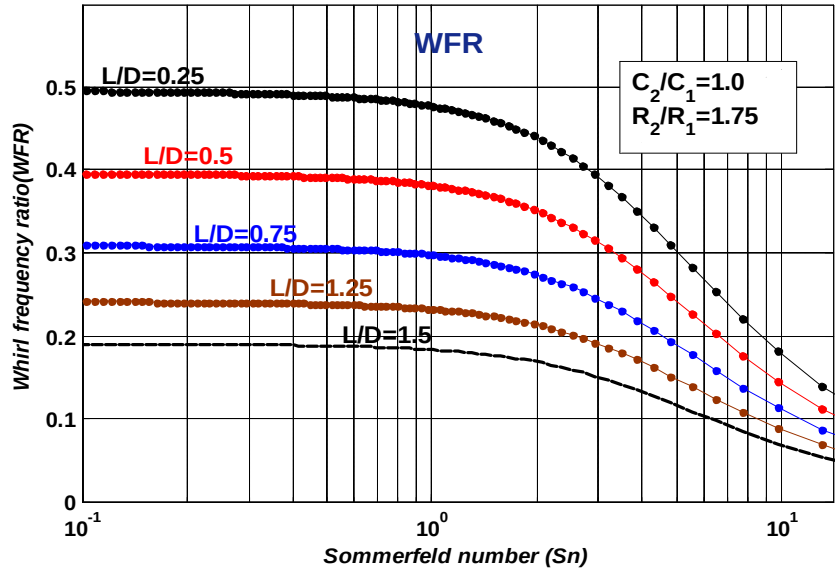

(a) *WFR* and slenderness for c_2/c_1=1.0

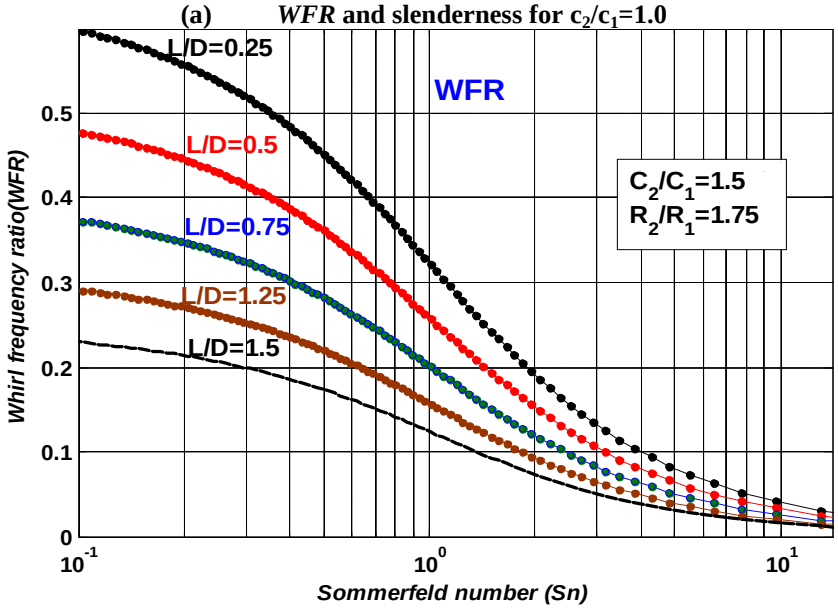

(b) *WFR* and slenderness for c_2/c_1=1.5

Fig. 7 Dependency of whirl frequency ratio on ring slenderness ratio for difference c_2/c_1

5.3 Predictions for Equivalent Force Coefficients of FRB

Figures 8 and 9 present the non-dimensional force coefficients plotted against the inner-film Sommerfeld number and journal eccentricity, respectively. The direct stiffness coefficient (K_{xx}) in the static load direction is higher at low Sn_1 (or high ε_1); but gradually drops in magnitude until it attains a fairly steady value of 4.03 for Sn_1>3.0 (or ε_1<0.1014). On the other hand, the value of K_{yy} changes from 3.57 at low Sn_1 to 4.02 for Sn_1>3.0. This implies that the FRB in the high-speed, stable region is symmetrically stiff, because the direct stiffness coefficients (K_{xx} , K_{yy}) are both equal. The prediction, also, shows that the direct stiffness terms (K_{xx} , K_{yy}) do not grow monotonically with increasing Sn_1, but reach limit values where further increase of Sn_1 does not produce noticeable changes in the former. Conversely, the cross-coupled stiffness terms (K_{xy}, K_{yx}) are significantly low compared to the direct terms, except for Sn_1>10 (or ε_1<0.03). This implies that a center-operating rotor could be unstable because of large K_{xy} and K_{yx} , particularly when there is inadequate damping effect.

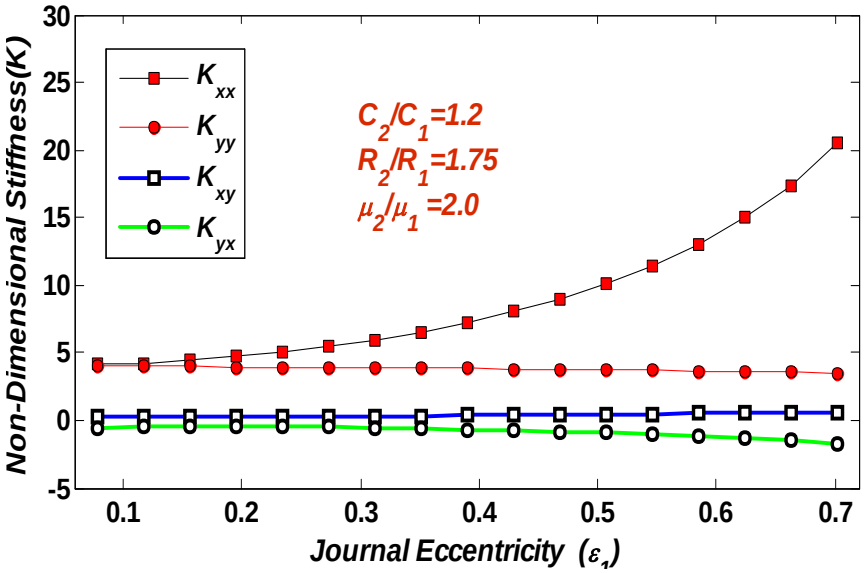

(a) Stiffness coefficients vs. journal eccentricity

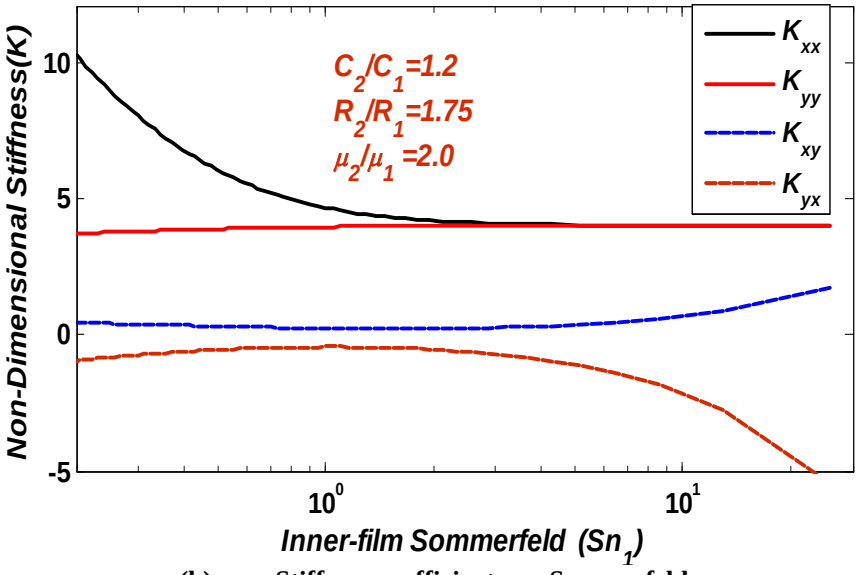

(b) Stiffness coefficients vs. Sommerfeld

Fig. 8 Predicted equivalent non-dimensional stiffness coefficients for FRB

Conversely, in Figures 9(a) and (b), the direct damping coefficients (Cxx, Cyy) are very sensitive to changes in Sn1 and ε1, especially for extremely low or high values. For instance, Cyy is very large in the range Sn1 ≥ 3.0. Such excellent damping effect precludes the possible occurrence of total rotordynamic instability in high-speed turbo rotor-bearing systems. Nonetheless, if eccentricity (ε1) reduces without an appreciable increase in Sn1, then total instability occurs because the destabilizing coefficients (Kxy, Kyx) are larger. This is likely for a lightly loaded rotor at center-operation. Note that total instability is not likely for heavily loaded, FRB-supported rotors operating at high speeds because of the excellent damping coefficients associated with their high Sn1. The analysis, also, shows that the cross-coupled damping terms (Cxy, Cyx) are generally very small and almost insensitive to changes in Sn1 and ε1.

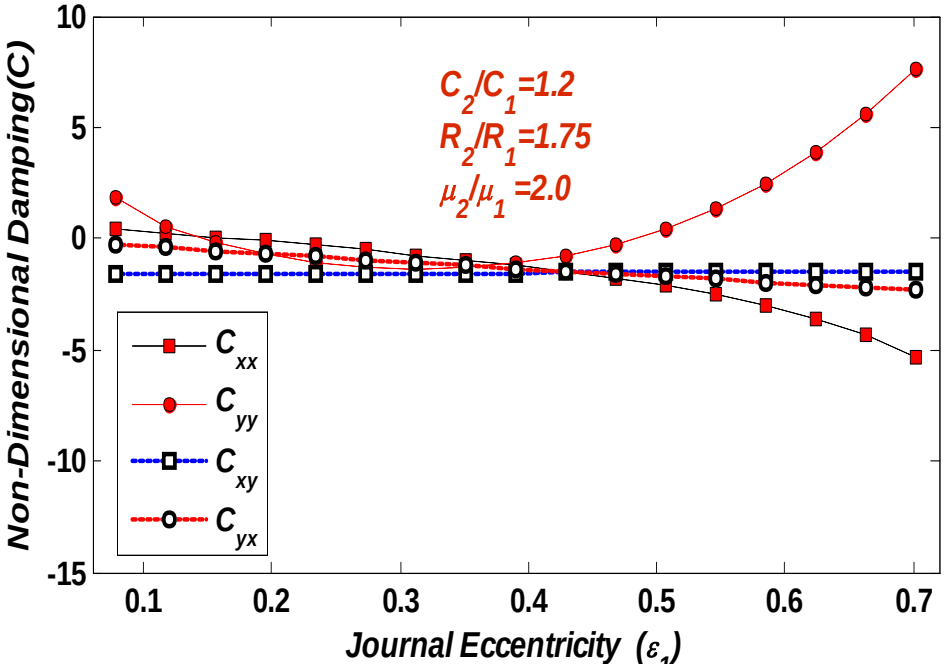

(a) Damping coefficients vs. journal eccentricity

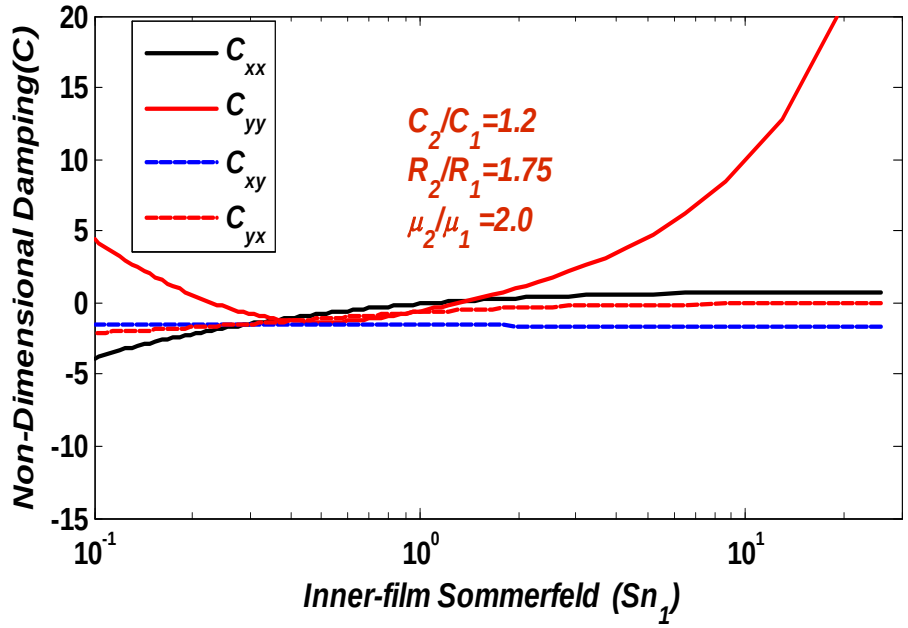

(a) Damping coefficients vs. Sommerfeld

Fig. 9 Predicted equivalent non-dimensional damping coefficients for FRB

5.4 Test data validation of Model Prediction of Ring-to-Journal Speed Ratio

Figure 10 displays the ring speed ratio by prediction plotted against measurement. The speed ratio decreases from 0.5 at Sn1= 0.1 to 0.06 at Sn1=10. This descent of N_2/N_1 is caused mainly by the increase in μ2/μ1. The values of N_2/N_1 predicted and measured are in good agreement. From the analysis: N_2/N_1 =0.1538 corresponds to Sn1= 2.927 (or ε1= 0.1014); and N_2/N_1 =0.3452 corresponds to Sn1= 0.8631 (or ε1=0.2886).

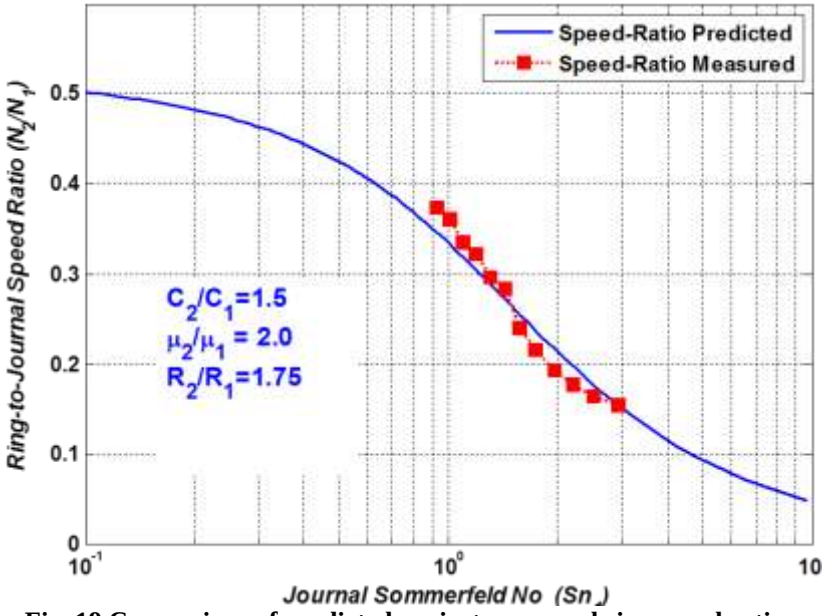

Fig. 19 Comparison of predicted against measured ring speed ratios

Note that the value of journal eccentricity relative to the ring is difficult to measure experimentally, since sensors cannot be attached directly on the floating-ring. By this comparison, the values of Sn_1 and ε_1 are easily determined. With this knowledge, the corresponding values for the outer-film Sommerfeld and ring eccentricity relative to the housing are readily estimated. The N_2/N_1 predicted virtually reproduces FRB test data, and validates the reliability of the model.

VI. CONCLUSION

This work models and predicts the thermo-hydrodynamic behavior of FRB applying modified Reynolds equation and incorporating thermo-viscous and centrifugal effects. Piecewise integration of film parameters for different FRB geometric ratios and operating conditions are implemented. The bearing force coefficients, ring-speed ratio, and stability characteristics are simulated and results adequately elucidated. The analysis shows that ring-speed ratio is largely influenced by viscosity thinning ($\mu 2/\mu 1 \rightarrow \infty$), especially at higher Sommerfeld number (Sn1> 10). Using a higher radius ratio R2/R1 only increases the inertia force: hence inducing significant impedance to the accelerating torque, particularly at low Sommerfeld number (Sn1 < 1.0). At high speeds (Sn1 > 10), the inertia effect on ring-speed becomes inconsequential. Only the viscous thinning effect subsists and governs over the ring-speed ratio. In contrast, changing clearance ratio (c2/c1) has weaker influence on NR/NJ, but impact significantly on stability characteristics of the rotor-bearing system. Furthermore, larger value of slenderness (L/D) enforces stability (i.e. WFR <0.5) of the rotor-bearing unit. This is greatly enhanced by a lower c2/c1. The model shows that the direct stiffness (Kxx) in the load direction is exponentially related to journal eccentricity (ε1). However, at high speed and low eccentricity, the bearing forces become more symmetric (Kxx ≈ Kyy). The rotordynamic stability is further improved by a corresponding large damping coefficient (Cyy). This implies that FRB supported rotor may wobble at low speed (Sn1<1.0) because of asymmetric film stiffness and low damping. Stability condition improves at high Sn1 making FRB most suitable for high-speed turbomachinery.

REFERENCES

[1] Shaw, C., and Nussdorfer, T., 1947, "An Analysis of the Full-Floating Journal Bearing," NACA Report No. 866, pp. 95-107
[2] Holt, C., San Andrés, L., Sahay, S., Tang, P., LaRue, G., and Gjika, K., 2005, "TestResponse and Nonlinear Analysis of a Turbocharger Supported on Floating Ring Bearings," ASME J. Vibr. Acoust., 127, pp. 1–9
[3] Tamunodukobipi, D., Kim, C.H., and Lee, Y.B., 2014, "Dynamic Performance Characteristics of Floating-Ring Bearings with Varied Oil-Injection Swirl-Control Angles," JDSMC of ASME Journals, doi: DS 13-1440
[4] Tanaka, M., and Hori, Y., 1972, "Stability Characteristics of Floating Bush Bearings," ASME J. Lubr. Technol., 94, pp. 248–259
[5] Tatara, A., 1970, "An Experimental Study on the Stabilizing Effect of Floating Bush Journal Bearings," Bull. JSME, 13, pp. 859–863
[6] Schweizer, B., 2009, "Total instability of turbocharger rotors — Physical explanation of the dynamic failure of rotors with full-floating ring bearings," Journal of Sound and Vibration, doi:10.1016/j.jsv.2009.03.028
[7] Chow, C.Y., 1983, "Dynamic Characteristics and Stability of a Helical Grooved Floating-Ring Bearing Operated in Turbulent Regime," ASLE Trans., 27(2), 154-63
[8] Orcutt, F., and Ng, C., 1968, Steady-State and Dynamic Properties of the Floating-Ring Journal Bearing, ASME J. Lubr. Technol.,

90, pp. 243–253
[9] Tamunodukobipi, D., Choe, B.S, and Lee, Y.B., 2014, "Feasibility Study of Instability Control of a Floating Ring Bearing for Turbocharger," Proceedings of Asian Congress on Gas Turbines, Seoul, Korea, ACGT2014-0156
[10] San Andrés, and Kerth, J., 2004, "Thermal Effects on the Performance of Floating Ring Bearings for Turbochargers," Proceedings of the Institution of Mechanical Engineers, Part J: J. Engineering Tribology, 218, pp. 1-14
[11] Tanaka, M., Hatakenaka, K. and Suzuki, K., "A Theoretical Analysis of Floating Bush Journal Bearing with Axial Oil Film Rupture Being Considered", Trans. ASME Journal of Tribology, Vol. 124, 2002, pp. 494-505
[12] Koeneke, C. E., Tanaka, M., and Motoi, H., 1995, "Axial Oil Film Rupture in High Speed Bearings Due to the Effect of the Centrifugal Force," ASME J. Tribol., 117, pp. 394–398
[13] Clarke, D. M., Fall, C., Hayden, G. N., and Wilkinson, T. S., 1987, "A steady-state model of a floating ring bearing, including thermal effects. Trans. ASME, J. Tribology, 1992, 114, 141–149
[14] Lee, Y. B., Park, D. J., Kim, C. H., and Kim, S. J., 2007, "Operating Characteristics of the Bump Foil Journal Bearings with Top Foil Bending Phenomenon and Correlation among Bump Foils," Tribology Int'l, triboint.2007.07.003, pp. 221 – 233.
[15] Childs, D. W., 1993, "Turbomachinery Rotordynamics: *Phenomena, Modeling and Analysis*," John Wiley & Sons, Inc., USA.
[16] Rao, J.S., 1996, Rotor Dynamics, New Age Int'l (P) Ltd, Daryaganj, New Delhi, India
[17] Hamrock, B. J., 1994, "Fundamentals of Fluid Film Lubrication," McGraw-Hill, Inc. Hightstown, NJ 08520, USA
[18] Pinkus, O., 1990, "Thermal Aspects of Fluid Film Tribology," ASME Press, New York.

Daniel Tamunodukobipi "Modeling and Analysis of Floating-Ring Bearing Thermo-Hydrodynamic Parameters for Advanced Turbo-Rotor Systems" American Journal of Engineering Research (AJER), vol. 6, no. 10, 2017, pp. 259-271